Quasiparticle Poisoning of Superconducting Qubits from Resonant Absorption of Pair-Breaking Photons

C. H. Liu,[1] D. C. Harrison,[2] S. Patel,[1] C. D. Wilen,[1] O. Rafferty,[1] A. Shearrow,[1] A. Ballard,[3] V. Iaia,[3] J. Ku,[3] B. L. T. Plourde,[3] and R. McDermott[1,*]

[1]Department of Physics, University of Wisconsin-Madison, Madison, Wisconsin 53706, USA
[2]Intelligence Community Postdoctoral Research Fellowship Program, Department of Physics, University of Wisconsin-Madison, Madison, Wisconsin 53706, USA
[3]Department of Physics, Syracuse University, Syracuse, New York 13244, USA

(Received 7 December 2022; revised 22 November 2023; accepted 29 November 2023; published 2 January 2024; corrected 24 January 2024)

The ideal superconductor provides a pristine environment for the delicate states of a quantum computer: because there is an energy gap to excitations, there are no spurious modes with which the qubits can interact, causing irreversible decay of the quantum state. As a practical matter, however, there exists a high density of excitations out of the superconducting ground state even at ultralow temperature; these are known as quasiparticles. Observed quasiparticle densities are of order 1 μm^{-3}, tens of orders of magnitude greater than the equilibrium density expected from theory. Nonequilibrium quasiparticles extract energy from the qubit mode and can induce dephasing. Here we show that a dominant mechanism for quasiparticle poisoning is direct absorption of high-energy photons at the qubit junction. We use a Josephson junction-based photon source to controllably dose qubit circuits with millimeter-wave radiation, and we use an interferometric quantum gate sequence to reconstruct the charge parity of the qubit. We find that the structure of the qubit itself acts as a resonant antenna for millimeter-wave radiation, providing an efficient path for photons to generate quasiparticles. A deep understanding of this physics will pave the way to realization of next-generation superconducting qubits that are robust against quasiparticle poisoning.

DOI: 10.1103/PhysRevLett.132.017001

In equilibrium, the ratio of thermally generated quasiparticles [1,2] to Cooper pairs in a superconductor x_{qp} is of order 10^{-50} at millikelvin temperatures. This is due to the exponential suppression of quasiparticle density with respect to the ratio of superconducting gap energy to temperature. Experimentally, however, x_{qp} is found to be more than 40 orders of magnitude larger than expected from the equilibrium calculation [3–8]. Nonequilibrium quasiparticles limit the sensitivity of superconducting devices for charge sensing [3,9], metrology [10], and astrophysical observation [11,12]. In the context of superconducting qubits, nonequilibrium quasiparticles represent a significant decoherence channel [1,5–8,13,14]. Recent experiments have demonstrated that quasiparticles liberated by particle impacts in the qubit substrate cause correlated errors in multiqubit arrays [15–18]. While such errors are especially damaging for quantum error correction, the particle impact rate is too low and the rate of removal of pair-breaking phonons in the aftermath of an impact is too high to account for the large baseline x_{qp} in superconducting quantum circuits.

Another potential source of quasiparticles is the absorption of pair-breaking photons. It has been shown that improvements in filtering and shielding can increase coherence times for superconducting resonators [19] and qubits [20]. Recently, Houzet *et al.* explained the observed ratio of the rate of charge-parity switches on the qubit island to the rate of qubit state transitions in terms of photon-assisted pair breaking at the Josephson junction; coupling of the photon to the qubit junction is mediated by higher-order modes of the qubit cavity [21]. Our group has put forth an alternate model for the resonant absorption of photons by spurious antenna modes of the qubit allowing detailed calculation of the spectral response [22]. The crucial insight is that the qubit structure exhibits a parasitic resonance at a frequency of order 100 GHz, set by the round-trip distance around the qubit island. This resonance is the aperture dual of the resonant wire loop antenna [23]. For typical qubit parameters, the qubit junction is well matched to free space via this antenna mode, so that the qubit is an efficient absorber of pair-breaking radiation. Figure 1(a) summarizes relevant quasiparticle generation and conversion mechanisms in superconducting qubits, while Fig. 1(b) depicts the dual mapping of the aperture antenna to wire antenna.

In this Letter, we describe the experimental validation of our model for the antenna coupling of qubits to pair-breaking radiation. The experiments involve two separate chips in one enclosure; one chip incorporates voltage-biased Josephson junctions acting as transmitters of

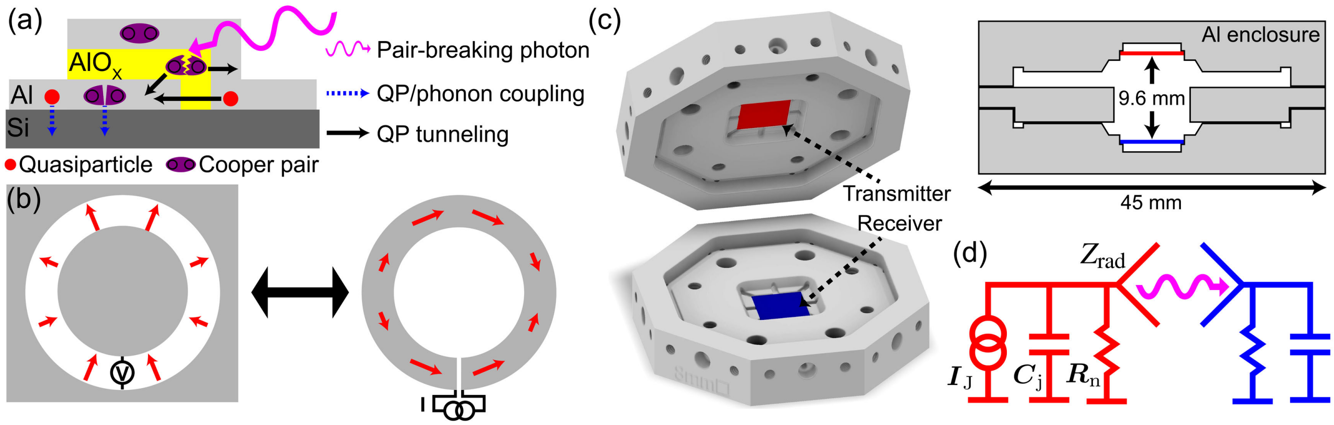

FIG. 1. Photon-assisted quasiparticle poisoning mediated by qubit's antenna modes. (a) Quasiparticle generation and conversion processes. Pair-breaking radiation is absorbed at a Josephson junction. Photon absorption changes the charge parity of the qubit island and can induce a qubit state transition. Quasiparticles couple to phonons through scattering and recombination. (b) The single-ended circular transmon (left) is the aperture dual of the resonant wire loop antenna (right). Red arrows show the amplitude and direction of electric fields. In the aperture(wire) antenna, signal is coupled via a high(low)-impedance source at the voltage(current) antinode [22]. (c) Two-chip transmit-receive geometry used to probe the spectral response of the qubits to mm-wave radiation. Cutaway drawing is a scale illustration of the sample enclosure. (d) Circuit diagram for the transmit-receive experiment, with mm-wave Josephson transmitter (red) and receiver qubit (blue).

coherent mm-wave photons, while the second chip supports superconducting qubits acting as receivers. We use a Ramsey-based interferometric gate sequence to monitor the charge-parity state of the qubits [24]; resonant absorption of pair-breaking photons induces parity switches on the qubit which we detect with near unit fidelity. By scanning the voltage bias of the transmitter junction, we map out the spectral response of the qubits up to ~500 GHz. We find that the detailed absorption spectrum of the qubits agrees well with the predictions. Additionally, we investigate the origin of the baseline quasiparticle poisoning and spurious excitation of the qubit.

We note that a recent experimental study explains the scaling of quasiparticle poisoning with qubit size in terms of our model, without direct validation of the detailed spectral response [25].

The experimental setup is shown in Fig. 1(c). Two separate device chips are integrated in a single light-tight enclosure made from 6061 aluminum: the transmitter chip (red) is mounted face to face with the receiver chip (blue) with a separation of 9.6 mm. Bias of the transmitter junction at voltage V induces coherent oscillations in the phase difference across the junction at the Josephson frequency $f_{\mathrm{J}} = V/\Phi_0$, where $\Phi_0 \equiv h/2e$ [26]. A circuit diagram of the experiment is shown in Fig. 1(d). Josephson oscillations are modeled within the resistively and capacitively shunted junction model [27] as a Norton equivalent current source I_{J} in parallel with shunt admittance $Y_{\mathrm{j}} = 1/Z_{\mathrm{j}} \approx 1/R_{\mathrm{n}} + j\omega C_{\mathrm{j}}$. Here, I_{J} is a frequency-dependent ac Josephson current of order the junction critical current I_0 [27–31], R_{n} is the differential resistance of the junction, and C_{j} is the junction capacitance. For a detailed discussion, see the Supplemental Material [32,33].

The Josephson oscillator acts as a coherent source that drives the antenna formed by the junction pads with radiation impedance Z_{rad}. The coherent power radiated to free space is given by [22]

$$P_{\mathrm{rad}} = \frac{e_{\mathrm{c,tr}}}{8} I_{\mathrm{J}}^2 R_{\mathrm{n}}, \tag{1}$$

where the coupling efficiency $e_{\mathrm{c,tr}}$ of the junction to free space is given by

$$e_{\mathrm{c,tr}} = 1 - \left| \frac{Z_{\mathrm{rad}} - Z_{\mathrm{j}}^*}{Z_{\mathrm{rad}} + Z_{\mathrm{j}}} \right|^2. \tag{2}$$

We now consider the effect of the radiation on the transmon qubits of the receiver chip. We use charge-sensitive transmons [14] to allow real-time monitoring of quasiparticle poisoning [33]. Photons with frequency $f > 2\Delta_{\mathrm{Al}}/h = 92$ GHz couple to the Josephson junction of the receiver qubit with efficiency $e_{\mathrm{c,rec}}$ defined as in Eq. (2). Photon absorption breaks a Cooper pair, resulting in a change in the charge parity of the qubit island.

In a first series of experiments, we use two nominally identical chips as transmitter and receiver. Witness junctions [shown in Fig. 2(a)] are used as mm-wave transmitters [41]. The chip incorporates six Xmon qubits; the qubit geometry is shown in Fig. 2(b). As we vary the voltage bias on the transmitter junction and thus the frequency of the emitted Josephson radiation, we probe the charge parity of the receiver qubit. In the following, we present data on a single transmitter-receiver pair [42].

In Fig. 2(c), we show the calculated coupling efficiencies e_{c} for the transmitter (red) and receiver (blue) [33]. The purple trace, the product of the transmitter and receiver efficiencies, represents the frequency-dependent transfer

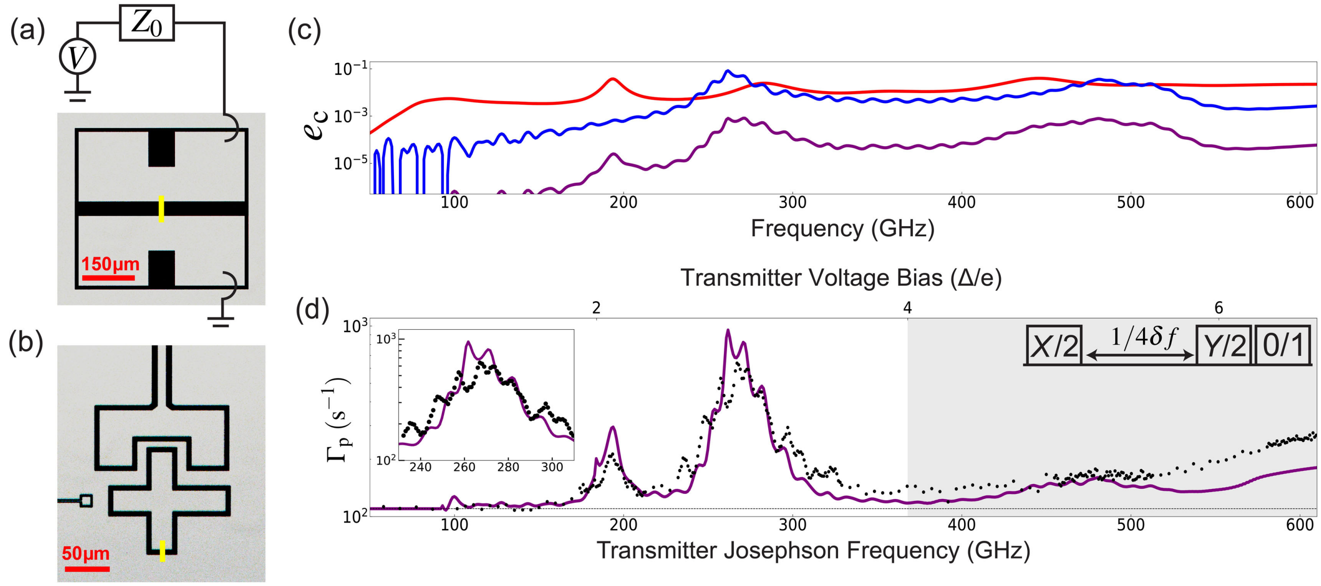

FIG. 2. Spectral response of the Xmon qubit. (a) Optical micrograph of the Josephson transmitter. Voltage bias is provided by a drive line with impedance $Z_0 = 50\ \Omega$. (b) Optical micrograph of the Xmon receiver qubit. In both (a) and (b), junction leads are shown in yellow. (c) Frequency-dependent coupling efficiency calculated for the transmitter junction (red) and receiver qubit (blue). The product of these coupling efficiencies (purple trace), represents the overall transfer efficiency from transmitter to receiver. (d) Quasiparticle poisoning rate as a function of transmitter frequency. Left: the parity-sensitive Ramsey sequence. Black points are the measured poisoning rates. The black dashed line is the baseline rate $\Gamma_0 = 110\ \mathrm{s}^{-1}$ (in the absence of explicit photon injection), and the purple trace is the contribution from Josephson radiation calculated from the coupling efficiencies of (c), with an overall scaling of 0.045 to account for photon losses. Right: a detailed view of the resonant features around 270 GHz. Oscillations in the spectral response of the qubit arise from the mutual coupling of the qubit antenna mode to a spurious slotline mode of the qubit readout resonator. Here and in the following, the shaded region on the right-hand side of the plot indicates the regime $V > 4\Delta_{\mathrm{Al}}/e$ where shot noise emission from the transmitter dominates over coherent emission.

function of the two-chip experiment in the absence of loss and nonidealities. In Fig. 2(d), we plot the measured parity switching rate Γ_p [43] of the receiver qubit versus transmitter Josephson frequency (black points). We see clear peaks in the spectral response of the receiver qubit at 190 GHz and 270 GHz, with Γ_p a factor of 2 and 6 times larger than the baseline rate, respectively. We ascribe these features to antenna resonances in our transmitter and receiver, which provide enhanced transfer of energy between the two chips. The purple trace represents the expected parity switching rate calculated from the coupling efficiencies [33].

In the inset of Fig. 2(d), we plot the measured and calculated parity switching rates on an expanded scale. We observe a clear fine structure in both spectra, with a modulation of the receiver response at a period of 11 GHz. We understand this modulation to be due to the mutual coupling between the receiver qubit and its local readout resonator [44]. We take the excellent agreement between the measured and calculated spectra as clear validation of our antenna model for coupling of the qubit to pair-breaking radiation.

For transmitter bias above $4\Delta_{\mathrm{Al}}/e = 0.76$ mV, corresponding to Josephson frequency above $8\Delta_{\mathrm{Al}}/h = 368$ GHz, shot noise from quasiparticles tunneling across the transmitter junction will also generate pair-breaking photons [45]. In the relevant limit $eV \gg 2\Delta_{\mathrm{Al}} \gg k_B T$, we can model shot noise from the transmitter as from a normal tunnel junction at zero temperature. We find an emitted power of pair-breaking radiation given by

$$P_{\mathrm{shot}}(f_J) = \frac{1}{4}\int_{2\Delta_{\mathrm{Al}}/h}^{f_J/2-2\Delta_{\mathrm{Al}}/h} \left[\frac{hf_J}{2} - hf\right] e_{c,\mathrm{tr}}(f)\,df, \quad (3)$$

where f_J is the frequency of coherent (Josephson) radiation corresponding to the junction voltage bias; see the Supplemental Material [33] for details. The upturn in the parity switching rate for Josephson frequency above ~400 GHz is well explained by this shot noise contribution.

In a second series of experiments, we examined the resonant response of receiver qubits with circular island geometry spanning a range of sizes; the geometries of the transmitter junction and the three receiver qubits are shown in Fig. 3(a). The devices are designed with the same nominal charging energy $E_c/h = 360$ MHz and ratio $E_J/E_c = 28$; however, the different island radii 90, 70, and 50 μm yield different dominant dipole antenna resonances at frequencies 130, 240, and 360 GHz, as confirmed by numerical modeling of the chip [Fig. 3(b)].

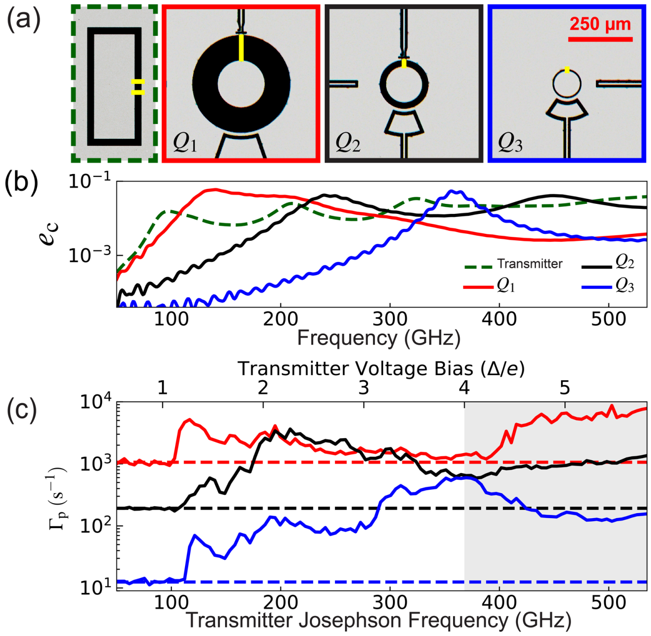

FIG. 3. Dependence of resonant response and baseline parity switching rate on device scale. (a) Optical micrographs of the rectangular transmitter device (green) and the large (red), intermediate (black), and small (blue) qubits used for these experiments. Yellow traces indicate the junction leads. (b) Calculated coupling efficiencies of the transmitter and the receiver qubits. (c) Measured quasiparticle poisoning rates for the qubits as a function of transmitter frequency. Dashed lines indicate the baseline parity switching rates.

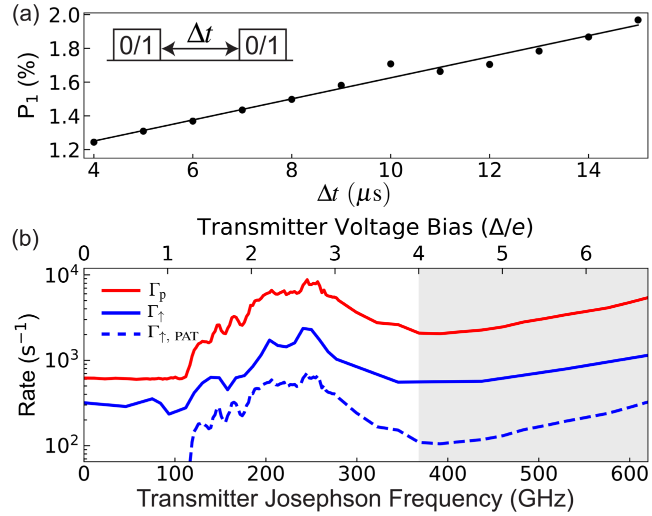

FIG. 4. Photon-assisted parity switches and qubit transitions. (a) Representative measurement of qubit excitation rate. Here we use qubit Q_2 as a testbed. Inset: the *measure-idle-measure* sequence. A linear fit (black line) is used to extract the excitation rate $\Gamma_\uparrow$. (b) Measured quasiparticle poisoning rate (red) and excitation rate (blue solid trace) as a function of transmitter frequency. The dashed curve shows the predicted photon-assisted qubit transition rate calculated from the measured rate of parity switches, after [21].

With the Josephson radiator turned off, we first measure the baseline parity switching rates on the three devices [dashed lines in Fig. 3(c)], finding $\Gamma_0(Q_1) = 1060\ \mathrm{s}^{-1}$, $\Gamma_0(Q_2) = 190\ \mathrm{s}^{-1}$, and $\Gamma_0(Q_3) = 12.8\ \mathrm{s}^{-1}$. The two orders of magnitude discrepancy in the baseline parity switching rates across these devices indicates clearly that nonequilibrium quasiparticles are not uniformly distributed on the receiver chip, and that device geometry plays a critical role in the generation of quasiparticles. If we take the radiative environment of the qubit to be a blackbody at effective temperature T and assume coupling of the qubit antenna to a single mode and polarization of the radiation field, we find a rate of absorption of pair-breaking photons given by

$$\Gamma_0 = \int \frac{e_c}{e^{hf/k_B T} - 1} df. \tag{4}$$

From the measured parity switching rates on the three devices, we infer effective blackbody temperatures $T(Q_1) = 410$ mK, $T(Q_2) = 490$ mK, and $T(Q_3) = 460$ mK. We believe that the broadband pair-breaking photons giving rise to the observed parity jumps are not due to a single radiator at a physical temperature of 400–500 mK, but rather due to light leakage from higher temperature stages of the refrigerator (most likely via the coaxial wiring) that is insufficiently attenuated by the in-line Eccosorb filters [25,46] and direct photon leakage into the sample box due to imperfect sealing of the enclosure. The discrepancy in the effective temperatures inferred for the 3 qubit antenna modes could reflect structure in the environmental spectrum.

With the transmitter junction biased in the voltage state, we map out the resonant response of these three devices as shown in Fig. 3(c). The complex resonant structure of the transmitter mode leads to rich structure in the resonant response of the 3 qubits; however, the measured parity switching rates are in qualitative agreement with our antenna model, with the resonant response shifting to higher frequency as the radius of the qubit island decreases.

Finally, using Q_2 as a testbed, we examine spurious transitions out of the qubit $|0\rangle$ state induced by the absorption of pair-breaking photons. In Fig. 4(a) we show representative data for the conditional probability $P_1 \equiv P(1|0)$ of finding the qubit in state $|1\rangle$ in the second measurement given the initial measurement prepared state $|0\rangle$. In Fig. 4(b), the solid traces show the measured parity switching rate Γ_p and excitation rate $\Gamma_\uparrow$ versus Josephson frequency of the transmitter junction. We see that Γ_p and $\Gamma_\uparrow$ display a similar resonant response centered at a Josephson frequency around 240 GHz, where the transfer function from transmitter to receiver device is expected to peak. Moreover, the ratio $\Gamma_p/\Gamma_\uparrow$ is roughly constant over the full frequency range, indicating that qubit excitations are dominated by resonant absorption of pair-breaking photons. Houzet *et al.* have previously analyzed the rate of qubit transitions conditioned on the absorption of a pair-breaking photon [21]. Their analysis predicts a contribution to $\Gamma_\uparrow$ given by the dashed blue trace in Fig. 4(b) [33]. However, the absorption of a pair-breaking photon will also generate a population of non-equilibrium quasiparticles that can tunnel across the qubit junction, inducing additional qubit transitions following the primary poisoning event. It is possible that this secondary poisoning accounts for the enhanced rate of excitations measured here.

In summary, we have used controlled irradiation of superconducting qubits with mm-wave photons derived from the ac Josephson effect to validate a model for photon-assisted quasiparticle poisoning through the spurious antenna modes of transmon qubits. The observed baseline parity switching rates are well explained by absorption of broadband thermal photons from higher temperature stages of the cryostat. Additionally, the correlation between qubit state transitions and charge parity switches indicates that resonant absorption of pair-breaking photons is the dominant contributor to qubit initialization errors in our devices.

An understanding of the physical origin of quasiparticle poisoning will allow the development of improved qubit designs and measurement configurations that protect against absorption of pair-breaking radiation. At the same time, the resonant transduction of pair-breaking photons to quasiparticles followed by qubit-based parity detection could form the basis for a new class of quantum sensors; potential applications include high-resolution spectroscopy of the cosmic microwave background [47] or detection of dark-matter axions [48,49] or dark energy [50].

Work at UW-Madison is supported by the Fermi National Accelerator Laboratory, managed and operated by Fermi Research Alliance, LLC under Contract No. DE-AC02-07CH11359 with the U.S. Department of Energy, through the Office of High Energy Physics QuantISED program. Work at Syracuse University is supported by the U.S. Government under ARO Grant No. W911NF-18-1-0106. We thank E. S. Joseph and M. Wolfe for assistance with device imaging. This research was supported by an appointment to the Intelligence Community Postdoctoral Research Fellowship Program at University of Wisconsin-Madison, administered by Oak Ridge Institute for Science and Education through an interagency agreement between the U.S. Department of Energy and the Office of the Director of National Intelligence. Portions of this work were performed at the UW-Madison Wisconsin Centers for Nanoscale Technology, partially supported by the NSF through the University of Wisconsin Materials Research Science and Engineering Center (DMR-1720415). Other portions were performed at the Cornell NanoScale Facility, a member of the National Nanotechnology Coordinated Infrastructure (NNCI), which is supported by the National Science Foundation under Grant No. NNCI-2025233.

*Corresponding author: rfmcdermott@wisc.edu

[1] G. Catelani, J. Koch, L. Frunzio, R. J. Schoelkopf, M. H. Devoret, and L. I. Glazman, Quasiparticle relaxation of superconducting qubits in the presence of flux, Phys. Rev. Lett. **106**, 077002 (2011).
[2] L. I. Glazman and G. Catelani, Bogoliubov quasiparticles in superconducting qubits, SciPost Phys. Lect. Notes **31**, 1 (2021).
[3] J. Aumentado, M. W. Keller, J. M. Martinis, and M. H. Devoret, Nonequilibrium quasiparticles and 2*e* periodicity in single-Cooper-pair transistors, Phys. Rev. Lett. **92**, 066802 (2004).
[4] M. Shaw, R. Lutchyn, P. Delsing, and P. Echternach, Kinetics of nonequilibrium quasiparticle tunneling in superconducting charge qubits, Phys. Rev. B **78**, 024503 (2008).
[5] J. M. Martinis, M. Ansmann, and J. Aumentado, Energy decay in superconducting Josephson-junction qubits from nonequilibrium quasiparticle excitations, Phys. Rev. Lett. **103**, 097002 (2009).
[6] U. Vool *et al.*, Non-Poissonian quantum jumps of a fluxonium qubit due to quasiparticle excitations, Phys. Rev. Lett. **113**, 247001 (2014).
[7] C. Wang *et al.*, Measurement and control of quasiparticle dynamics in a superconducting qubit, Nat. Commun. **5**, 5836 (2014).
[8] P. J. De Visser, J. J. Baselmans, J. Bueno, N. Llombart, and T. M. Klapwijk, Fluctuations in the electron system of a superconductor exposed to a photon flux, Nat. Commun. **5**, 3130 (2014).
[9] E. T. Mannila, P. Samuelsson, S. Simbierowicz, J. T. Peltonen, V. Vesterinen, L. Grönberg, J. Hassel, V. F. Maisi, and J. P. Pekola, A superconductor free of quasiparticles for seconds, Nat. Phys. **18**, 145 (2022).
[10] D. M. T. vanZanten, D. M. Basko, I. M. Khaymovich, J. P. Pekola, H. Courtois, and C. B. Winkelmann, Single quantum level electron turnstile, Phys. Rev. Lett. **116**, 166801 (2016).
[11] P. Day, H. LeDuc, B. Mazin, V. Anastasios, and J. Zmuidzinas, A broadband superconducting detector suitable for use in large arrays, Nature (London) **425**, 817 (2003).
[12] P. M. Echternach, B. J. Pepper, T. Reck, and C. M. Bradford, Single photon detection of 1.5 THz radiation with the quantum capacitance detector, Nat. Astron. **2**, 90 (2018).
[13] S. Gustavsson *et al.*, Suppressing relaxation in superconducting qubits by quasiparticle pumping, Science **354**, 1573 (2016).
[14] K. Serniak, M. Hays, G. deLange, S. Diamond, S. Shankar, L. D. Burkhart, L. Frunzio, M. Houzet, and M. H. Devoret, Hot nonequilibrium quasiparticles in transmon qubits, Phys. Rev. Lett. **121**, 157701 (2018).
[15] A. P. Vepsäläinen *et al.*, Impact of ionizing radiation on superconducting qubit coherence, Nature (London) **584**, 551 (2020).
[16] C. D. Wilen *et al.*, Correlated charge noise and relaxation errors in superconducting qubits, Nature (London) **594**, 369 (2021).
[17] M. McEwen *et al.*, Resolving catastrophic error bursts from cosmic rays in large arrays of superconducting qubits, Nat. Phys. **18**, 107 (2021).

[18] V. Iaia, J. Ku, A. Ballard, C. P. Larson, E. Yelton, C. H. Liu, S. Patel, R. McDermott, and B. L. T. Plourde, Phonon downconversion to suppress correlated errors in superconducting qubits, Nat. Commun. **13**, 6425 (2022).

[19] R. Barends, H. L. Hortensius, T. Zijlstra, J. J. A. Baselmans, S. J. C. Yates, J. R. Gao, and T. M. Klapwijk, Contribution of dielectrics to frequency and noise of NbTiN superconducting resonators, Appl. Phys. Lett. **92**, 223502 (2008).

[20] A. D. Córcoles, J. M. Chow, J. M. Gambetta, C. Rigetti, J. R. Rozen, G. A. Keefe, M. B. Rothwell, M. B. Ketchen, and M. Steffen, Protecting superconducting qubits from radiation, Appl. Phys. Lett. **99**, 181906 (2011).

[21] M. Houzet, K. Serniak, G. Catelani, M. H. Devoret, and L. I. Glazman, Photon-assisted charge-parity jumps in a superconducting qubit, Phys. Rev. Lett. **123**, 107704 (2019).

[22] O. Rafferty *et al.*, Spurious antenna modes of the transmon qubit, arXiv:2103.06803.

[23] C. A. Balanis, *Antenna Theory: Analysis and Design* (Wiley, New York, 2016).

[24] D. Ristè, C. C. Bultink, M. J. Tiggelman, R. N. Schouten, K. W. Lehnert, and L. DiCarlo, Millisecond charge-parity fluctuations and induced decoherence in a superconducting transmon qubit, Nat. Commun. **4**, 1913 (2013).

[25] X. Pan *et al.*, Engineering superconducting qubits to reduce quasiparticles and charge noise, Nat. Commun. **13**, 7196 (2022).

[26] M. C. Cassidy, A. Bruno, S. Rubbert, M. Irfan, J. Kammhuber, R. N. Schouten, A. R. Akhmerov, and L. P. Kouwenhoven, Demonstration of an ac Josephson junction laser, Science **355**, 939 (2017).

[27] K. K. Likharev, *Dynamics of Josephson Junctions and Circuits* (Gordon and Breach, New York, 1986).

[28] A. Barone and G. Paterno, *Physics and Applications of the Josephson Effect* (Wiley, New York, 1982).

[29] N. R. Werthamer, Nonlinear self-coupling of Josephson radiation in superconducting tunnel junctions, Phys. Rev. **147**, 255 (1966).

[30] R. E. Harris, Cosine and other terms in the Josephson tunneling current, Phys. Rev. B **10**, 84 (1974).

[31] R. E. Harris, Experimental demonstration of the Riedel peak, Phys. Rev. Lett. **26**, 426 (1971).

[32] The IV characteristic of an underdamped Josephson junction is highly nonlinear for bias around the gap voltage $2\Delta/e$, corresponding to $f_J = 184$ GHz for these experiments. For simplicity, here we take the real part of the junction admittance to be $1/R_n$ over the full frequency span, not only for bias above the gap. Our modeling shows that reduced quasiparticle conductance in the subgap region will lead to a reduction in emission efficiency for bias below the gap. However, separate measurements show that strong coupling of the transmitter junction to its low-impedance environment will suppress the hysteresis in the junction IV characteristic and lead to higher subgap conductance approaching $1/R_n$. See the Supplemental Material [33] for a detailed discussion.

[33] See the Supplemental Material at http://link.aps.org/supplemental/10.1103/PhysRevLett.132.017001, which includes Refs. [34–40] for further modeling and analysis of transmit-receive experiment.

[34] G. J. Dolan, Offset masks for liftoff photoprocessing, Appl. Phys. Lett. **31**, 337 (1977).

[35] D. J. Scalapino and T. M. Wu, Radiation-induced structure in the dc Josephson current, Phys. Rev. Lett. **17**, 315 (1966).

[36] U. Eckern, G. Schön, and V. Ambegaokar, Quantum dynamics of a superconducting tunnel junction, Phys. Rev. B **30**, 6419 (1984).

[37] CST Studio Suite, www.3ds.com.

[38] A. F. Clark, G. E. Childs, and G. H. Wallace, Electrical resistivity of some engineering alloys at low temperatures, Cryogenics **10**, 295 (1970).

[39] V. Ambegaokar, U. Eckern, and G. Schön, Quantum dynamics of tunneling between superconductors, Phys. Rev. Lett. **48**, 1745 (1982).

[40] S. B. Kaplan, C. C. Chi, D. N. Langenberg, J. J. Chang, S. Jafarey, and D. J. Scalapino, Quasiparticle and phonon lifetimes in superconductors, Phys. Rev. B **14**, 4854 (1976).

[41] One pad of the transmitter is connected to the chip ground plane via a short wirebond, while the opposite pad is bonded to the 50 Ω bias line. Detailed modeling of the chip geometry using CST Microwave [37] reveals that loading of the transmitter antenna with the wirebond and 50 Ω drive line only slightly modifies the radiation impedance of the structure. See the Supplemental Material [33] for a detailed discussion.

[42] All three of the receiver qubits studied on this chip displayed a similar spectral response; see the Supplemental Material [33] for more details.

[43] See Eq. S1 and the surrounding discussion in the Supplemental Material [33] for details.

[44] The readout resonator involves a spurious $\lambda/2$ slotline mode at a frequency that is roughly twice that of the $\lambda/4$ coplanar waveguide resonance at 6.058 GHz.

[45] M. Frey and H. Grabert, Effect of the electromagnetic environment on current fluctuations in driven tunnel junctions, Phys. Rev. B **94**, 045429 (2016).

[46] K. Serniak, S. Diamond, M. Hays, V. Fatemi, S. Shankar, L. Frunzio, R. J. Schoelkopf, and M. H. Devoret, Direct dispersive monitoring of charge parity in offset-charge-sensitive transmons, Phys. Rev. Appl. **12**, 014052 (2019).

[47] Z. Wang, M. Xu, X. Han, W. Fu, S. Puri, S. M. Girvin, H. X. Tang, S. Shankar, and M. H. Devoret, Quantum microwave radiometry with a superconducting qubit, Phys. Rev. Lett. **126**, 180501 (2021).

[48] A. V. Dixit, S. Chakram, K. He, A. Agrawal, R. K. Naik, D. I. Schuster, and A. Chou, Searching for dark matter with a superconducting qubit, Phys. Rev. Lett. **126**, 141302 (2021).

[49] T. Braine *et al.* (ADMX Collaboration), Extended search for the invisible axion with the axion dark matter experiment, Phys. Rev. Lett. **124**, 101303 (2020).

[50] S. Ghosh, E. P. Ruddy, M. J. Jewell, A. F. Leder, and R. H. Maruyama, Searching for dark photons with existing haloscope data, Phys. Rev. D **104**, 092016 (2021).

Correction: The previously published Fig. 4(b) contained an error in the color curve key and has been replaced.